ACADEMIC PRESS

Available online at www.sciencedirect.com
SCIENCE DIRECT®

Journal of Catalysis 218 (2003) 111–122

JOURNAL OF CATALYSIS

www.elsevier.com/locate/jcat

On the structure sensitivity of deNO$_x$ HC-SCR over Pt-beta catalysts

J.M. García-Cortés,[a] J. Pérez-Ramírez,[b] J.N. Rouzaud,[c] A.R. Vaccaro,[d] M.J. Illán-Gómez,[a] and C. Salinas-Martínez de Lecea [a,*]

[a] *Department of Inorganic Chemistry, University of Alicante, P.O. Box 99, E-03080, Alicante, Spain*
[b] *Hydrocarbon Processes and Catalysis, Oil & Energy Research Centre, Norsk Hydro, P.O. Box 2560, N-3907, Porsgrunn, Norway*
[c] *Centre de Recherche sur la Matière Divisée, 1B, rue de la Férollerie, 45071 Orléans Cédex 2, France*
[d] *Reactor & Catalysis Engineering, DelftChemTech, Delft University of Technology, Julianalaan 136, 2628 BL Delft, The Netherlands*

Received 19 October 2002; revised 15 January 2003; accepted 21 February 2003

Abstract

In this paper, the integration of activity results for the selective catalytic reduction of NO_x with C_3H_6 with a thorough characterization of Pt-beta catalysts with different platinum dispersion has been accomplished. The parent zeolite NH_4-beta (Si/Al = 11.4) was ion-exchanged with a Pt(II) precursor and activated by calcination and reduction in H_2 before reaction. The evolution and nature of the Pt phase during the different preparation stages and after catalytic tests were investigated by CO chemisorption, TEM, XRD, and XPS. By using different heating rates during activation of the ion-exchanged material and upon the deNO$_x$ HC-SCR, the average particle size of platinum in the final catalyst was varied in the range of 2–25 nm. It has been clearly shown that deNO$_x$ HC-SCR conditions produce a decrease in the metal dispersion of the catalysts by sintering of Pt particles. The increase in average particle size has a positive effect on the activity of the catalysts. Thus, the larger the platinum particles, the higher the NO_x conversion and the lower the operation temperature. The XPS results show that both Pt(0) and Pt(II) species are present in the calcined samples, after H_2 reduction and during reaction. Coke deposits, formed during reaction on the zeolite support, were studied by XPS, DRIFT, and TPO-TPD/MS. The structure sensitivity of the lean deNO$_x$ reaction toward the platinum phase has been confirmed by the direct correlation established between platinum particle size and TOF. Based on previous results on a single crystal, it seems that the key steps are the NO dissociation on Pt(100) planes and Pt–O clean off which will be easily performed on large Pt particles. On the other hand, the independence of Pt(100)/Pt(111) ratios with particle size explains the similar N_2 and N_2O selectivity values presented along all the samples.

Keywords: Pt; Beta; DeNO$_x$; SCR; C_3H_6; Structure sensitive; Particle size; Coke; Activation; Sintering; Dispersion

1. Introduction

At low temperatures (200–250 °C), platinum catalysts show a high activity and stability for the selective catalytic reduction of NO_x with hydrocarbons (HC-SCR) even under adverse reaction conditions such as the presence of water and SO_2 [1–5]. Therefore, these catalysts are attractive for eliminating NO_x, e.g., from car exhaust streams containing excess oxygen (lean deNO$_x$ process). The influence of the support on the deNO$_x$ activity and N_2 selectivity over Pt-catalysts was previously investigated by some of the authors [5]. The order of activities found was Pt-USY > Pt/activated carbon > Pt-ZSM-5 > Pt/Al_2O_3 > Pt/SiO_2. A similar Pt loading in catalysts was used, but the properties of the support and the metal dispersion varied simultaneously. This made it very difficult to establish a correlation between the activity observed and the metal dispersion, since acidic properties of the support seems to play an essential role in hydrocarbon activation and thus in the overall catalytic performance. Even though no definitive correlation was found, it seemed that high metal dispersions were not attractive to achieve a high activity.

Several authors have investigated the influence of the dispersion on the performance of platinum catalysts for various reactions. The structure sensitivity of processes catalyzed by Pt has been typically reported in (1) the reduction of NO by H_2 [6] or CH_4 [7,8], (2) the oxidation of NO with O_2 [9], and (3) the combustion of hydrocarbons (e.g.,

* Corresponding author.
E-mail address: c.salinas@ua.es (C. Salinas-Martínez de Lecea).

0021-9517/03/$ – see front matter
doi:10.1016/S0021-9517(03)00088-5

propene, methane, and chlorobenzene) [10]. In some cases there is an increase of reaction rate with increasing in Pt particle size. Burch et al. [4] presented an apparent hyperbolic relation between dispersion of the fresh catalyst and turnover frequency (TOF) for NO reduction with hydrocarbons on Pt/Al_2O_3 and Pt/SiO_2 systems.

Several studies on Pt/Al_2O_3 have suggested that NO might aid the sintering of small platinum particles. Denton et al. [11] combined HC-SCR activity measurements with characterization of fresh and used Pt/Al_2O_3 and Pt/SiO_2 catalysts. Based on H_2 chemisorption and TEM analysis of fresh and used catalysts it was concluded that on meso, macro, and nonporous support materials, platinum particles smaller than 3 nm are not stable under reaction conditions and undergo sintering. Only on microporous silica supports, dispersions $> 30\%$ were preserved upon reaction. Lööf et al. [12] showed that treatment with 0.1 vol% NO in Ar effectively induced sintering of small reduced platinum particles (< 2 nm) over Pt/Al_2O_3 already at relatively low temperature ($\geqslant 473$ K). This effect was confirmed by Schneider et al. [13] using X-ray absorption spectroscopy. The same authors found no sintering in mixtures of NO and O_2 (500 ppm NO and 14 vol% O_2 in N_2), while it occurred when the reducing agent was added to the mixture (500 ppm NO, 500 ppm C_3H_6, and 14 vol% O_2 in N_2) [14].

The influence of platinum dispersion on the HC-SCR performance was also studied over zeolitic supports. Xin et al. [15] prepared Pt-ZSM-5 catalysts with different average particle sizes by variation of activation conditions and found higher turnover frequencies in Pt-ZSM-5 catalysts with lower dispersion. However, the structural changes of the platinum phase due to reaction were not analyzed. Contrarily, Shin et al. [16] characterized a Pt-ZSM-5 catalyst and found a bimodal platinum particle-size distribution with maxima at 3 and 13 nm. Changes in the particle size distribution of the used catalyst due to sintering upon $deNO_x$ HC-SCR were observed, but changes in TOF were not assessed by the authors.

Previous studies lack a detailed combination of activity and characterization data to derive conclusive explanations on the structure sensitivity of Pt catalysts in $deNO_x$ HC-SCR. Both aspects have been integrated in this paper, using Pt-beta as the catalyst. To the best of our knowledge, this catalytic system has not been reported for the reaction under investigation. Beta zeolite has been selected as a catalyst support regarding its acidity, relatively open structure, and thermostability. This study contributes to a better understanding of the evolution of the platinum phase upon the $deNO_x$ reaction, enabling a correlation with the performance observed.

For this purpose, preparing Pt catalysts with a controlled dispersion using the same support is essential for overcoming the difficulties of previous studies, when metal dispersion and support were changed simultaneously. A method for preparing Pt-beta catalysts with different platinum particle size, based on previous work by Creyghton et al. [17], has been successfully applied. By changing the heating rate during activation (calcination and reduction in H_2) of the ion-exchanged Pt-beta and upon $deNO_x$ HC-SCR, Pt catalysts with a wide range of dispersions, from 4 to 47%, were obtained. Following this approach, the relative difference of $deNO_x$ HC-SCR performance can be strictly related to the metallic phase, since the zeolitic support is invariable.

The catalysts were subjected to activity tests under different conditions. The effect of catalyst activation and ageing conditions during reaction on the dispersion, morphology, and oxidation state of the platinum phase was investigated by CO chemisorption, HRTEM, XRD, and XPS. The location of coke deposits was analyzed by DFTIR, XPS, and TPO-TPD/MS. Based on this, structure–activity relationships have been derived which contribute to the understanding of the structure sensitivity of the $deNO_x$ HC-SCR process.

2. Experimental

2.1. Catalyst preparation

The parent zeolite NH_4-beta was supplied by Zeolyst (CP814E) with a molar SiO_2/Al_2O_3 ratio of 25 and a total surface area of 680 $m^2\,g^{-1}$. Pt-beta catalysts were prepared by a conventional aqueous ion-exchange method. The nominal metal content was 1 wt% Pt. The exchange was carried out under vigorous stirring at 295 K for 18 h, using diluted aqueous solutions (0.30 mM) of tetraammineplatinum(II) nitrate, $[Pt(NH_3)_4](NO_3)_2$, and a solid-to-liquid ratio of 1 $g\,L^{-1}$. The ion-exchanged zeolite was then filtered and washed thoroughly with deionized water at room temperature before drying at 385 K for 12 h.

The dry ion-exchanged zeolite, denoted as Pt-beta(*ie*), was calcined in static air at 400 °C for 2 h, using four different heating rates, i.e., 0.5, 2, 5, and 10 °C min^{-1}. The calcined samples are denoted as Pt-beta(*c*-*x*), where *x* is the heating rate applied. Previous to the activity tests, the catalysts were reduced at 350 °C in pure H_2 atmosphere for 8 h (100 ml min^{-1}), using the same corresponding heating rate as in the calcination step (denoted as Pt-beta(*r*-*x*)).

2.2. Catalyst characterization

The chemical composition of Pt-beta(*ie*) was determined by inductive coupled plasma-optical emission spectroscopy (ICP-OES) (Perkin-Elmer Plasma 40 (Si) and Optima 3000DV (axial)) and atomic absorption spectroscopy (AAS) (Perkin-Elmer 1100).

The platinum dispersion was determined by CO chemisorption using a volumetric apparatus (QuantaChrome Autosorb-1C). The experimental error is lower than 10%. Prior to the measurement, the samples were treated in pure hydrogen at 200 °C, using the lowest possible heating rate (1 °C min^{-1}) to minimize sintering effects. Based on the

amount of CO adsorbed and assuming an adsorption stoichiometry CO:Pt = 1:1, the metal dispersion was obtained. The average Pt particle size was calculated by applying the following equation [18],

$$D = Ag/\delta\theta N d_s,$$

where D is metal dispersion in the catalyst, A is atomic weight of the active atoms, g is shape factor ($g = 6$ for hemispherical geometry of the metal particles), δ is metal density, θ is cross-sectional area of active atom (8.0 Å^2 per atom), N is Avogadro's number, and d_s is average particle size.

A Philips CM 20 microscope, operating at 200 kV, was used to obtain the HRTEM images of the catalysts. Samples were mounted on a copper grid-supported carbon film by placing a few droplets of an ultrasonically dispersed suspension of sample in ethanol on the grid, followed by drying at ambient conditions. TEM images were obtained by using both low- and high-energy electron beam and were analyzed with an image analysis procedure (Sigma ScanPro 5), in order to semiquantitatively determine the average Pt particle size.

Powder X-ray diffraction (XRD) was used for the detection of crystalline phases in the catalysts. The measurements were carried out in a Bruker-AXS diffractometer using a diffracted beam graphite monochromator and Cu-K_α radiation. The patterns were collected in the 2θ range of 5 to 75° with a step size of 0.1° 2θ and a counting time of 8 s. In order to improve the signal-to-noise ratio of the Pt reflections, some of the catalysts were measured in $2\theta = 35$–50°, using a step size of 0.02° 2θ and a counting time of 20 s.

XPS was carried out in a VG-Microtech Multilab electron spectrometer by using Mg-K_α (1253.6 eV) radiation source. To obtain the XPS spectra, the pressure of the analysis chamber was maintained at 5×10^{-10} mbar. The binding energy (BE) and the kinetic energy (KE) scales were adjusted by setting the C1s transition at 284.6 eV. The BE and KE values were determined with the software Peak-fit of the spectrometer. The characteristic BE corresponding to the core levels of Pt $4f_{7/2}$ and $4f_{5/2}$ included in Table 1 were used for fitting the Pt photoemissions lines.

Fourier transform infrared (FT-IR) spectra were recorded under ambient conditions without any pretreatment using a Spectratech diffuse reflectance (DRIFT) accessory and a Nicolet Magna 550 Fourier transform spectrometer. The spectral range was 400–4000 cm^{-1} and they were recorded by coaddition of 256 scans (scanning time in 300 s), with a nominal resolution of 4 cm^{-1}.

Table 1
Characteristic binding energies (BE in eV) of Pt $4f_{7/2}$ and $4f_{5/2}$

	Pt $4f_{7/2}$	Pt $4f_{5/2}$
Pt(0)	71.3	74.6
Pt(II)	72.7	76.1

TPO-TPD/MS experiments with the used catalysts were carried out in a Mettler-Toledo TGA-SDTA 851 apparatus equipped with a sample robot and a gas controller for air or inert gas (He). The solid (∼ 10 mg sample, no dilution) was placed in an alumina crucible (70 µl) using α-Al_2O_3 as reference. Tests were performed in a dry air (TPO) or a helium (TPD) flow of 100 cm^3(STP) min^{-1} at atmospheric pressure. The temperature was increased from 25 to 500 °C with a heating rate of 10 °C min^{-1}. For the experiment in inert gas, a prepurge step in He (100 cm^3(STP) min^{-1}) at room temperature was applied to remove the remaining air in the reaction chamber. The evolution of the gases during these experiments was analyzed on line by a computer-controlled quadrupole mass spectrometer (Pfeiffer Thermostar). The microbalance and the spectrometer were coupled through a heated capillary sampling tube.

2.3. Activity tests

DeNO$_x$ HC-SCR activity measurements were carried out in a quartz-tube fixed-bed reactor of 10-mm i.d. and 35-mm bed height at atmospheric pressure. About 250 mg of catalyst (125–250 µm) was used for each run and the total flow rate was 100 ml(STP) min^{-1} (GHSV = 15,000 h^{-1}). After in situ reduction of the catalysts (pure H_2, 100 ml(STP) min^{-1}, 350 °C, 12 h) at a specific heating rate, temperature was decreased to the desired value and the feed mixture was passed through the catalyst. The feed mixture contained 1000 ppm NO_x, 1500 ppm C_3H_6, 5 vol% O_2 with He as balance gas. Two types of experiments were carried out over reduced catalysts: (i) *steady-state activity*, consisting in point-by-point isothermal reaction experiments in the range of 100–500 °C using the same heating rate as in the calcination and reduction steps (generally 2 h after a change of conditions, the conversion levels for the different gases were constant and considered as the steady state); and (ii) *stability*, consisting in time-on-stream experiments for 30 h at the maximum activity temperature. Experiment (i) yielded a catalyst used at relatively high temperature (500 °C) (Pt-beta(*ht-x*)), and experiment (ii) yield a catalyst used at lower temperature (Pt-beta(*lt-x*)). Finally, in order to check the possible catalyst activation, samples Pt-beta(*ht-x*) were cooled down and submited to a new steady-state activity test (experiment (i)).

The product gases were continuously analyzed with a chemiluminescence NO–NO_2 analyzer (Signal 4000 VM), and discontinuously analyzed for the other gases by a gas chromatograph (HP 6890). The chromatograph was equipped with a thermal conductivity detector, using two serial columns (Porapak Q 80/100, for CO_2, C_3H_6, N_2O, and H_2O separation, and a Molecular Sieve 13X, for O_2, N_2, and CO separation).

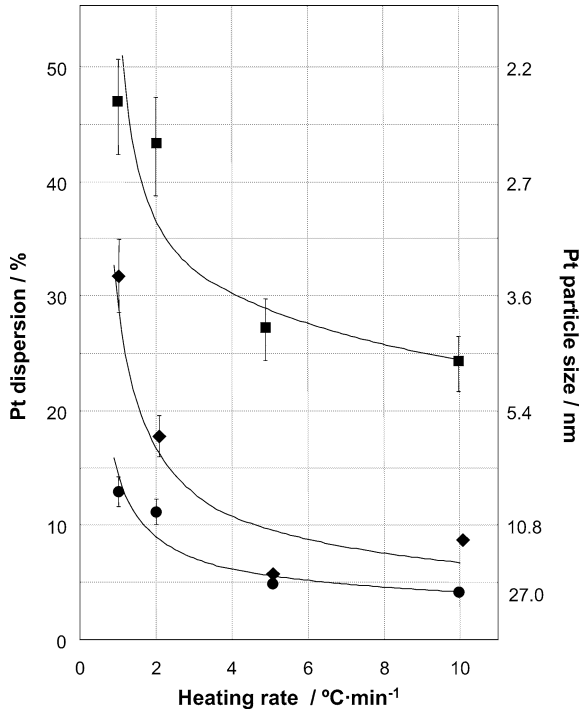

Fig. 1. Pt dispersion and particle size (determined from CO chemisorption) as a function of heating rate for (■) Pt-beta(*r*), (◆) Pt-beta(*lt*), and (●) Pt-beta(*ht*) catalysts.

3. Results and discussion

3.1. Influence of the heating rate during activation on the Pt dispersion

The ion-exchanged Pt-beta(*ie*) zeolite, with a platinum content of 0.92 wt%, was activated in static air at 400 °C using four different heating rates (0.5, 2, 5, and 10 °C min^{-1}) and subsequently reduced in H_2 flow at 350 °C using the same heating rates. The metal dispersion and the average particle size determined from CO chemisorption are shown in Fig. 1. The platinum dispersion in the catalysts decreases with increasing heating rate, upon calcination and reduction.

At low heating rates relatively high Pt dispersions are achieved ($\sim$ 50%), in agreement with previous studies [10, 19,20]. Due to equipment specifications the minimum heating rate used for reduction previous to CO chemisorption was limited to 1 °C min^{-1}. A variation of heating rate from 2 to 5 °C min^{-1} produces a considerable decrease of Pt dispersion from 43 to 27%, i.e., the average Pt particle size increases from 2.5 to 4.0 nm. However, a minor change in Pt dispersion at higher heating rates is identified, indicating that it is difficult to achieve very low Pt dispersion just by increasing the heating rate. It is well known that the velocity of the sintering process strongly depends on the actual size distribution of the metal particles. With small particles sintering is fast, with bigger particles it is slow [21].

CO chemisorption provides an average platinum particle size within the limits imposed by an uncertain stoichiometry [18]. On zeolitic supports, structure and morphology of the platinum phase are potentially more complex than on base metal oxides. Metal or metal oxide particles at the external surface of the zeolite crystal may coexist with isolated platinum ions at ion-exchange positions and/or oligonuclear species PtO_x located in the zeolite channels; e.g., the formation of microcrystalline PtO on calcined Pt-faujasite prepared by ion-exchange was unambiguously detected by Chmelka et al. [22], who used Raman spectroscopy to characterize the platinum species. Since hydrogen easily reduces these PtO species, zero-valent platinum atoms produced finally form small metal clusters inside or outside the microporous network [17].

For the purpose of this research, an extensive analysis by transmission electron microscopy is required to have a direct measurement of the Pt particle-size distribution in the different catalysts. HRTEM micrographs of reduced Pt-beta catalysts typically show a relatively broad distribution of Pt particle sizes, which gives an idea of the heterogeneous nature of the metallic phase on the zeolite support. Platinum particles with a size of < 2 nm prevail in Pt-beta(*r*-2) (Fig. 2a). Using a low-intensity electron beam at high magnification (Fig. 2b), the zeolite lattice can be clearly distinguished, although it is not clear if Pt clusters are located in the zeolite channels (see region within the circle in the micrograph). In addition, some Pt particles in a broad distribution from 5 to 50 nm can be also identified in the catalyst. These particles are likely to be located at the external surface of the zeolite crystal.

The particle-size distribution in the samples reduced at high heating rates (5 or 10 °C min^{-1}) appears to be quite similar to the samples reduced at low heating rates (0.5 and 2 °C min^{-1}). However, the average platinum particle size is larger in the samples at higher heating rates, as can be seen for Pt-beta(*r*-10) in Fig. 3. This result also substantiates the effect of the heating rate to favor the sintering of platinum particles during reduction in H_2 of the calcined catalysts. The average Pt particle size determined from the TEM micrographs using an image analysis procedure was in good agreement with that obtained from CO chemisorption.

3.2. Catalytic activity

The catalytic performance for the NO_x reduction with propene of Pt-beta(*r*-10) is shown in Fig. 4a as an example of the typical behavior of Pt-beta samples. NO_x conversion increases with temperature passing through a maximum when propene conversion 1 is reached. By definition the NO_x conversion summarizes the conversion of NO and NO_2 to N_2 and N_2O. As can be observed in Fig. 4b, NO_2 coexists with NO at temperatures with full propene conversion, which is beyond the maximum NO_x conversion. Therefore only NO reduction reactions for NO_x conversion are considered in our discussion.

Attending to N_2 selectivities, Fig. 4a includes N_2 selectivity which is similar than other platinum-based catalysts reported in the literature [1,5], N_2O is an important product

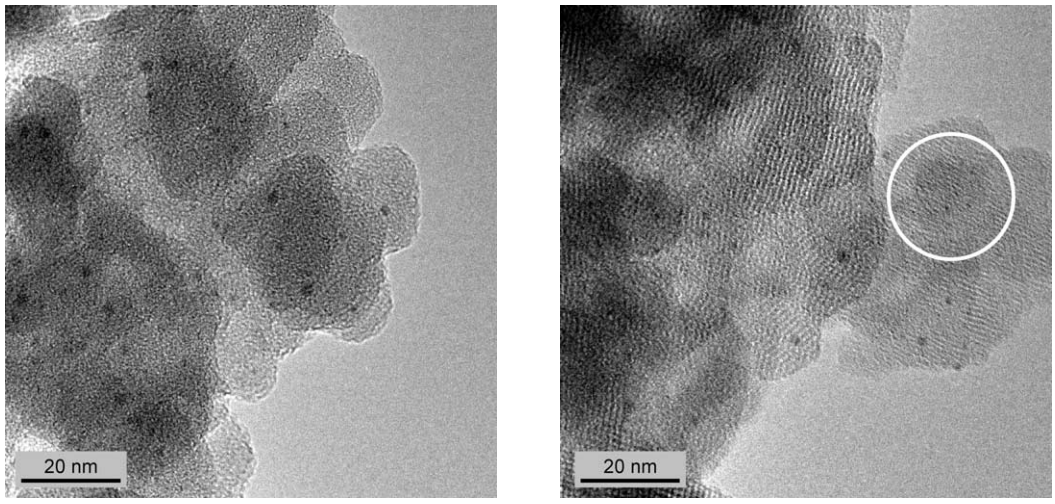

(a) (b)

Fig. 2. TEM micrographs of Pt-beta(*r*-2) using (a) high-energy and (b) low-energy beam. See detailed procedures in the text.

of the deNO$_x$ reaction over Pt-beta catalysts. At temperatures below the maximum NO$_x$ conversion, the N$_2$ selectivity was ∼ 35%. At higher temperatures, as expected, the N$_2$ selectivity increases with temperature.

This catalytic behavior can be understood considering the reactions involved during deNO$_x$ HC-SCR process [23]. The competitive reactions that take place are

$$\mathrm{NO} + \mathrm{C_3H_6} + 4\mathrm{O_2} \rightarrow \tfrac{1}{2}\mathrm{N_2} + 3\mathrm{CO_2} + 3\mathrm{H_2O}, \quad (1)$$

$$2\mathrm{NO} + \mathrm{C_3H_6} + 4\mathrm{O_2} \rightarrow \mathrm{N_2O} + 3\mathrm{CO_2} + 3\mathrm{H_2O}, \quad (2)$$

$$\mathrm{C_3H_6} + \tfrac{9}{2}\mathrm{O_2} \rightarrow 3\mathrm{CO_2} + 3\mathrm{H_2O}, \quad (3)$$

$$\mathrm{NO} + \tfrac{1}{2}\mathrm{O_2} \leftrightarrow \mathrm{NO_2}. \quad (4)$$

At temperatures below 150 °C, the NO$_x$ concentration corresponds to that introduced initially (see Fig. 4b). At temperatures in the range of 200–250 °C NO reduction by C$_3$H$_6$ [reactions (1) and (2)] is activated in parallel to the total combustion of C$_3$H$_6$ [reaction (3)]. In this range, the ratio between NO$_x$ and propene conversion, defined as the hydrocarbon efficiency, $E(\mathrm{HC}) = X(\mathrm{NO}_x)/X(\mathrm{C_3H_6})$, is close to 1. With increasing temperature, the fraction of propene consumed by reaction (3) increases at the expense of reactions (1) and (2). As a result, the NO$_x$ conversion drops when temperature is further increased beyond that of complete C$_3$H$_6$ conversion and the E(HC) continuously decreases. At temperatures in the range of 250–300 °C the decreasing NO reduction [reactions (1) and (2)] is fully mirrored by a net increase in NO oxidation [reaction (4)] as it is indicated by the constant NO level (see Fig. 4b). Finally, at higher temperatures, reaction (4) is limited by its thermodynamic equilibrium.

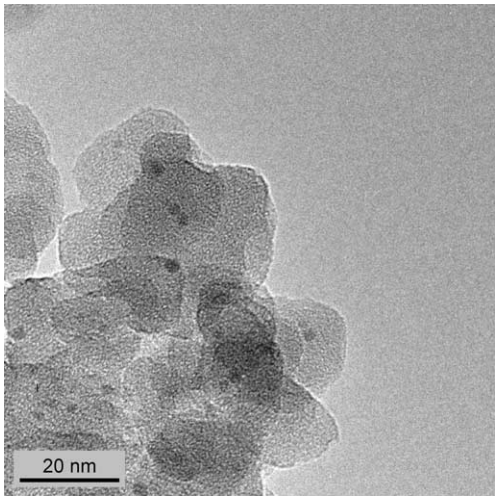

Fig. 3. TEM micrograph of Pt-beta(*r*-10).

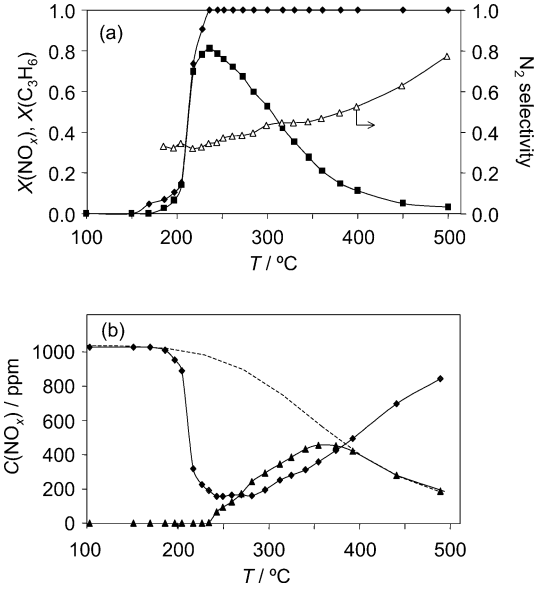

Fig. 4. (a) Conversion of (■) NO$_x$, (◆) C$_3$H$_6$, and (△) N$_2$ selectivity vs temperature over Pt-beta(*r*-10) and (b) corresponding concentration profiles of (◆) NO and (▲) NO$_2$ vs temperature during deNO$_x$ C$_3$H$_6$-SCR. Equilibrium composition of NO$_2$ is represented by dashed lines. Experimental conditions: 1000 ppm NO, 1500 ppm C$_3$H$_6$, 5 vol% O$_2$, balance He; $P = 1$ bar; GHSV = 15,000 h^{-1}.

Table 2
Maximum conversion of NO_x and C_3H_6 during HC-SCR over the catalysts and the corresponding N_2 selectivity and peak temperature

	T_{max}	Conversion		N_2
	(°C)	NO_x	C_3H_6	selectivity
Pt-beta(*r*-0.5)	250	0.70	1	0.31
Pt-beta(*r*-2)	240	0.75	1	0.35
Pt-beta(*r*-5)	220	0.80	1	0.34
Pt-beta(*r*-10)	235	0.80	1	0.32
Pt-beta(*lt*-0.5)	249	0.74	1	0.34
Pt-beta(*lt*-2)	238	0.79	1	0.32
Pt-beta(*lt*-5)	218	0.86	1	0.35
Pt-beta(*lt*-10)	234	0.85	1	0.35
Pt-beta(*ht*-0.5)	245	0.78	1	0.35
Pt-beta(*ht*-2)	235	0.84	1	0.31
Pt-beta(*ht*-5)	218	0.91	1	0.32
Pt-beta(*ht*-10)	232	0.91	1	0.33

Table 2 collects relevant results of the activity tests. Pt-beta effectively reduces NO_x using C_3H_6 as reducing agent. The NO_x levels show the typical values for Pt-supported catalysts, surpassing 0.70 at temperatures below 250 °C. An effect of the Pt dispersion is observed; the maximum NO_x conversion increases and the peak temperature decreases as Pt dispersion goes down. The N_2 selectivity values are close to 35% and no effect of dispersion is observed.

Stability tests during 30 h showed no deactivation of Pt-beta(*lt-x*) catalysts (Table 2), and performance along exposure time was stable. On the contrary, the catalysts were activated as maximum activity levels were slightly increased corresponding to slightly lower peak temperatures. Typical N_2 and N_2O selectivities of $\sim$ 35 and 65% were achieved, respectively. This indicates no effect of platinum dispersion on the product distribution which is in agreement with the conclusions obtained by Denton et al. [11] using different supports for Pt catalysts.

With the purpose of studying the effect of higher temperatures on the performance of the catalysts, the samples used for steady-state activity tests (see Experimental) were cooled from 500 to 150 °C and subjected to a second steady-state activity test. As can be observed in Table 2 (Pt-beta*(ht-x)*) a significant increase on the NO_x conversion, and a peak temperature decrease, is achieved in all the cases. This point will be discussed later.

3.3. Sintering of platinum during deNO_x HC-SCR

Fig. 1 also shows the Pt dispersion and particle size from CO chemisorption of the catalysts used in deNO_x HC-SCR (Pt-beta(*lt-x*) and Pt-beta(*ht-x*)). The platinum dispersion of the catalysts is further decreased compared to the calcined and reduced catalysts. The reaction at high temperature (500 °C) induces a more severe platinum sintering. However, more important than the temperature itself is the effect of the reaction atmosphere. Despite of the fact that the Pt-beta(*lt-x*) catalysts were tested at lower temperatures ($\sim$ 200 °C) than those corresponding to calcination and reduction (400–350 °C) of Pt-beta(*ie*), the dispersion considerably decreases during the reaction. These observations are consistent with previous results reported for Pt/Al_2O_3 [12–14]. A possible explanation for the metal dispersion decrease in the reaction mixture is the eventual coke formation (detectable with the naked eye), covering the metal particles and decreasing the amount of CO adsorbed. This point will be analyzed in detail later.

As noted for the fresh catalysts, the presence of big platinum particles (> 50 nm) was also observed in TEM micrographs of the used catalysts, but they are a minority and its size has not significantly grown during different heat treatments. However, small particles in the region $\leqslant$ 2 nm suffered a particle-size increase proportional to that found in CO chemisorption experiments. The TEM micrograph of Pt-beta(*lt*-2) and Pt-beta(*ht*-2) (Figs. 5a and b, respectively),

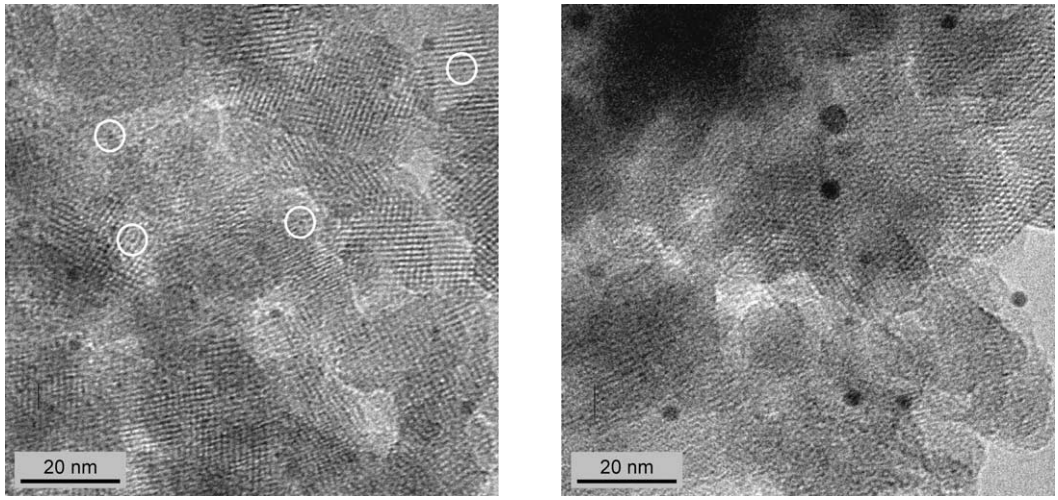

(a) (b)

Fig. 5. TEM micrographs of (a) Pt-beta(*lt*-2) and (b) Pt-beta(*ht*-2) using a low-energy electron beam.

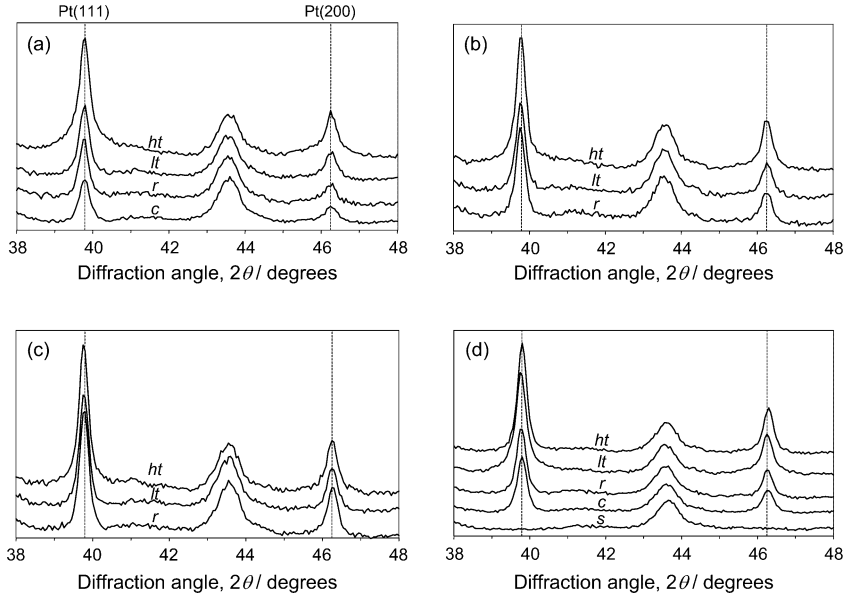

Fig. 6. XRD patterns for fresh and used samples (a) Pt-beta(x-0.5), (b) Pt-beta(x-2), (c) Pt-beta(x-5), and (d) Pt-beta(x-10).

clearly show a progressive sintering of Pt particles during reaction, as compared to Pt-beta(*r*-2) in Fig. 2b.

XRD experiments were also carried out to study the evolution of the crystalline platinum phase in the catalysts upon different treatments. Fig. 6 shows the patterns of the different samples, which have been normalized toward reflection of the parent zeolite support at 43.5° 2θ (Fig. 6d). Besides the typical reflections of beta, all samples present reflections at 39.7 and 46.2° 2θ, which are characteristic of metallic platinum. This enables us to follow the relative intensity of Pt-metal reflections after reduction in hydrogen and the deNO$_x$ SCR reaction. Reflections typical for crystalline Pt oxides were completely absent. Any form of Pt oxide on the samples would be either amorphous or too small to be XRD visible.

In most cases, the Pt metal reflections are sharp, indicating the presence of relatively large metal particles, as confirmed by TEM analysis. In other cases line broadening indicates the presence of smaller platinum particles being big enough to affect the XRD signal. Note that in case of line broadening both Pt metal reflections are equally affected, so instrumental errors or additional reflections are highly improbable causes for this phenomenon.

Taking into account that metal particles below 2 nm do not contribute to the XRD reflections, the intensity increase of the platinum reflection without peak broadening strongly indicates the formation of additional XRD-visible platinum metal particles at the expense of XRD-invisible (small) platinum particles. On the other hand, the peak broadening indicates that newly created very small visible XRD platinum metal particles arise from invisible ones. The metal in the freshly reduced catalyst Pt-beta(*r*-0.5) was highly dispersed and consequently a large fraction of particles are not visible by XRD. Peak broadening is especially observed in Pt-beta(*ht*-0.5), which exhibits the larger sintering process (see Fig. 1).

The ion-exchanged zeolite and the catalysts prepared at 0.5 and 5 °C min^{-1} have also been analyzed by XPS. Fig. 7 shows the Pt 4*f* spectra of these samples. Pt(0) and Pt(II) peaks are present in all the samples, except in Pt-beta(*ie*) (only Pt(II)). Table 3 collects the binding energies, obtained from the corresponding spectra, as well as the Pt surface concentration and the Pt(0) and Pt(II) surface concentration obtained from the data referred to the major element in the catalysts, i.e., oxygen.

In general, the Pt surface concentration on the catalysts as obtained by XPS significantly differs from that of the bulk composition according to ICP/OES (0.92 wt%). This deviation is a function of the metal dispersion. During calcination (400 °C, 2 h) of the ion-exchanged sample, the Pt concentration at the catalyst surface diminishes by $\sim$ 10%. An even more pronounced loss of Pt concentration is observed after the succeeding thermal treatment (reduction at 350 °C, 8 h). When the lowest heating rate was used for heat treatment steps, samples showed a higher dispersion. Used samples present lower values of Pt surface concentration, with a more marked effect for the catalyst used at high temperature (500 °C), i.e., Pt-beta(*ht*-0.5) and Pt-beta(*ht*-5). In general, these results are in agreement with CO chemisorption, HRTEM, and XRD.

The different Pt species found with XPS represent different structures. The Pt(0) signal clearly belongs to metallic Pt particles. The Pt(II) signal may represent isolated ions on ion-exchange positions (e.g., $[Pt(NH_3)_4]^{2+}$ and Pt^{2+}), or small nanoparticle being fully or partially oxidized. Not surprisingly, Pt(II) was the only Pt species found on the ion-exchanged sample. In agreement with the literature [20,24] and our XRD data shown in Fig. 6a, XPS data indicate that even during calcination at the lowest heating rate, a fraction

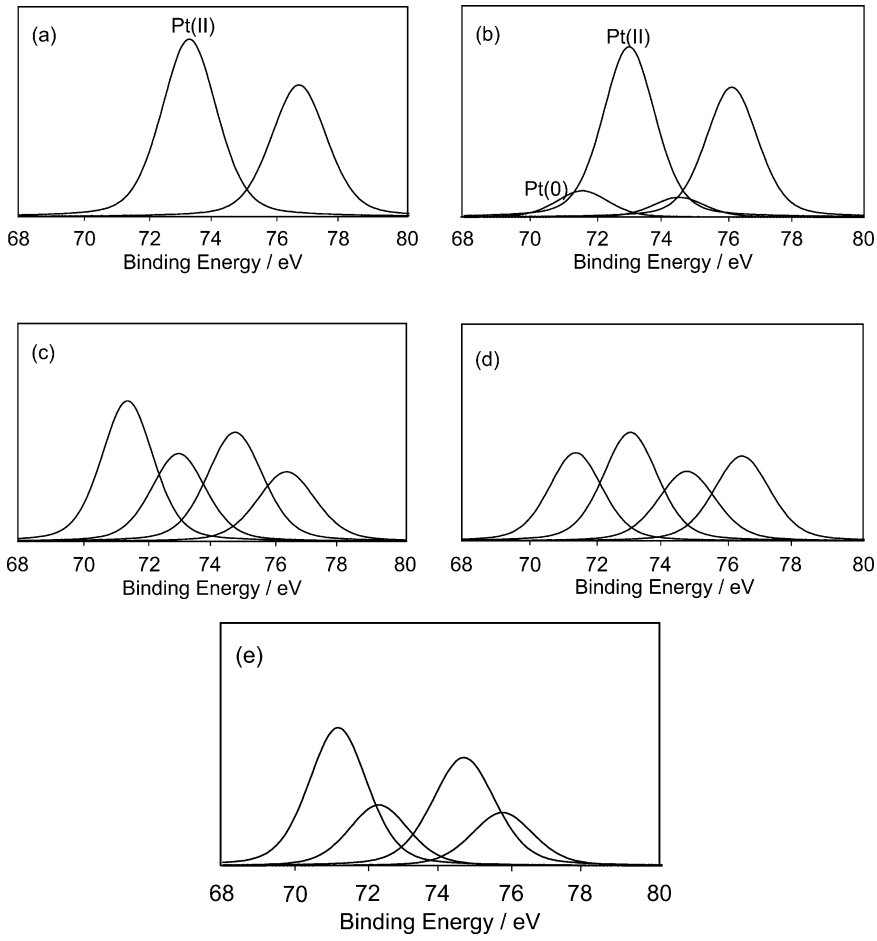

Fig. 7. Pt 4*f* XPS spectra for (a) Pt-beta(*ie*), (b) Pt-beta(*c*-0.5), (c) Pt-beta(*r*-0.5), (d) Pt-beta(*lt*-0.5), and (e) Pt-beta(*ht*-0.5).

Table 3
Summary of XPS results

Sample	BE Pt(0) (eV)	BE Pt(II) (eV)	Pt surface (wt%)	Pt(0) surface (wt%)	Pt(II) surface (wt%)
Pt-beta(*ie*)	–	73.20	0.75	0	0.75
Pt-beta(*c*-0.5)	71.48	73.00	0.65	0.08	0.57
Pt-beta(*r*-0.5)	71.35	72.95	0.48	0.29	0.19
Pt-beta(*lt*-0.5)	71.50	72.90	0.45	0.20	0.25
Pt-beta(*ht*-0.5)	71.10	72.20	0.40	0.28	0.12
Pt-beta(*c*-5)	71.48	73.00	0.68	0.14	0.54
Pt-beta(*r*-5)	71.12	72.61	0.37	0.18	0.19
Pt-beta(*lt*-5)	71.32	72.97	0.38	0.14	0.24
Pt-beta(*ht*-5)	71.59	73.14	0.34	0.17	0.17

of the Pt(II) species present in the ion-exchanged zeolite is reduced to Pt(0). The presence of Pt(0) has been attributed by Creyghton et al. [17] to the reduction of Pt(II) by the ammonia ligands of the Pt precursor removed during calcination.

The reduction step further reduces Pt(II) to Pt(0). However, an important amount of Pt still remains in an oxidized state. Significant concentrations of Pt(II) in reduced Pt catalysts have also been found by other authors, even after an in situ reduction [25]. The authors have justified this due to the difficult reducibility of the small oxidic platinum particles in the zeolite microporous network, which is evidence of a strong interaction between Pt and the zeolite support. Moreover, EXAFS analysis of samples exposed to air revealed that platinum nanoparticles of ~ 1 nm are completely oxidized, whereas particles of a few nanometers are partially oxidized [20].

The effect of the heating rate is mainly related to the Pt(0) value and not to the Pt(II) value, which could indicate that the structure of the phase belonging to Pt(0) is determined by kinetics, whereas the structure of the phase belonging to Pt(II) is determined by a thermodynamic equilibrium.

The stability test procedure (Pt-beta(*lt*-*x*)) decreases the surface concentration of Pt(0), but increases the Pt(II) concentration. Remarkably, the concentration of Pt(II) is the same for both Pt-beta(*lt*-*x*) samples, which could point again to a thermodynamic equilibrium. Spending at high temperatures keeps the amount of Pt(0) species almost stable, but decreases the amount of Pt(II) species. Considering the total Pt surface decrease observed, this represents a net transformation of Pt(II) species into metallic Pt.

Our results, in agreement with other obtained with different supports, i.e., Al_2O_3 and SiO_2 [11], reveal that, during selective catalytic reduction of NO_x using C_3H_6, the platinum particles sinter on the Pt-beta catalysts. The effect of

sintering in catalyst activity will be discussed in the last section.

According to the mechanism proposed by García-Cortés et al. [5], Pt surfaces adsorb NO under reaction conditions, which is further dissociated, generating a layer of atomic oxygen and atomic nitrogen being a precursor for N_2 and N_2O formation. Propene would act as a clean-off agent removing atomic oxygen generated by NO and O_2. Here, the formation of Pt metal appears to be essential for the reaction. As a consequence, Pt(II) species found on the various samples are considered as being inactive for HC-SCR, whereas Pt(0) represents active species.

3.4. Coke formation during HC-SCR

The presence of black spots in the spent catalysts was clearly identified. They correspond to coke deposits, as confirmed by comparing the C1*s* XPS spectra of Pt-beta(*r*-0.5) and Pt-beta(*lt*-0.5) (Fig. 8). The spectrum of Pt-beta(*lt*-0.5) shows a signal close to 281 eV, which is absent in the spectrum of Pt-beta(*r*-0.5). A direct and accurate identification of the C1*s* transition cannot be achieved at these binding energies, since different assignments are possible. In aluminosilicate-supported catalysts, some authors have found bands at similar binding energies, which are assigned to C–H-type species in the support, i.e., C–Al and C–Si type bonds [26,27]. Several authors have also assigned these signals to C–C and C=C bonds, characteristic of carbides and coke [27–29]. Since no evidence of coke deposits on Pt particles in the used catalysts was found from HRTEM or of Pt–C interactions in the Pt 4*f* XPS spectra of these samples, it is concluded that coke is preferentially formed on the bulk of the zeolite. The absence of deactivation of Pt-beta catalysts during deNO_x HC-SCR (general for platinum catalysts) also supports the idea that coking does not occur on Pt particles, but on the support.

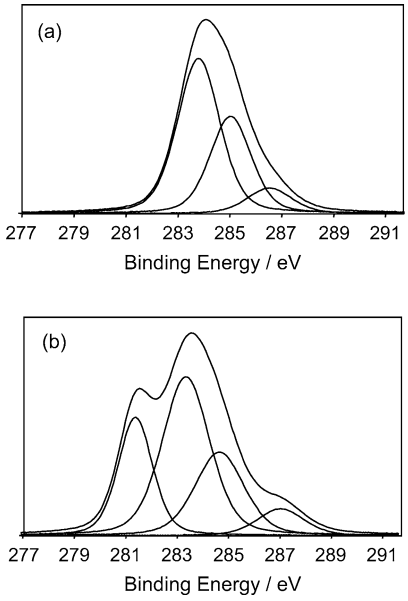

Fig. 8. C1*s* XPS spectra of (a) Pt-beta(*r*-0.5) and (b) Pt-beta(*lt*-0.5).

Ex situ DRIFT experiments were also carried out over the more representative samples to substantiate the former statements. Fig. 9 shows these spectra in a range of 800–2000 cm^{-1}. Pt-beta(*c*-0.5) and Pt-beta(*r*-0.5) show a very similar spectra and the bands identified are attributed to the zeolite framework and to physically adsorbed water [30]. However, H-beta and Pt-beta(*ie*) show an additional broad band at ~ 1450 cm^{-1}. This band, which disappears after calcination (in beta(*c*-10) and Pt-beta(*c*-0.5)), can be assigned either to allylic C–C–C species and C–H-bending vibrations, whose origin could be the zeolite Si precursor (TEOS), the template used during the synthesis of the zeolite, or to N–H bands on NH_4^+ ions present in the parent zeolite [30].

In the used catalysts, additional bands can be identified at 1580 and 1470 cm^{-1}. Again, it is difficult to do the spectral assignment of these bands because there are numerous assignments in the literature for bands in these positions [31–34]. Between 1570 and 1590 cm^{-1}, carbonates, carboxylates, and formates (C=O vibrations), nitrates and organo-nitrates (N=O vibrations), and also aromatic coke (C=C stretching) have been identified [30–33]. Bands around 1470 cm^{-1} have been attributed to nitro- complexes, carbonates, carboxylates, and formates and allylic species C–C–C and C–H-bending vibrations [30–33]. Since no sample showed additional absorption bands in the range between 2900 and 3200 cm^{-1}, the presence of C–H bonds cannot be definitively proven. In a similar way to XPS, and keeping in mind that these experiments have been carried out ex situ, the bands observed should correspond to long-life species. So, reaction intermediates like ($C_xH_yO_z$) are not likely to be responsible for these bands. In our opinion, such

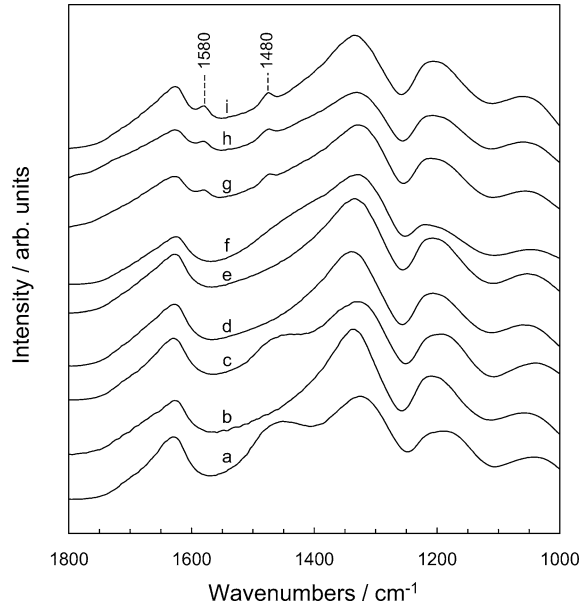

Fig. 9. Ex situ FT-IR spectra: (a) H-beta, (b) beta(*c*-10), (c) Pt-beta(*ie*), (d) Pt-beta(*c*-0.5), (e) Pt-beta(*r*-0.5), (f) Pt-beta(*ht*-10), (g) Pt-beta(*ht*-0.5), (h) Pt-beta(*lt*-10), and (i) Pt-beta(*lt*-0.5).

bands can be assigned to coke formed during reaction, i.e., C=C stretching and/or C–C–C vibrations [30]. Other authors have also assigned these bands in zeolites aged in gas engine exhausts to highly unsaturated carbonaceous residues or coke [34].

Temperature-programmed experiments in oxidizing (air, TPO mode) or inert (He, TPD mode) conditions were also used to study the nature of these deposits. This method is specifically suited to quantify coke deposits in the catalyst, by following the combustion products [35]. Fig. 10a shows the H_2O and CO_2 signals during TPO experiments over Pt-beta(*c*-0.5). Desorption of physically adsorbed water takes place at 100 °C. Mass m/e 44, corresponding to CO_2, does not vary along the temperature range investigated. In the TPO profile of Pt-beta(*lt*-0.5) (Fig. 10b), a significant amount of CO_2 (m/e 44) is generated (with a maximum at 345 °C) without additional H_2O desorption in parallel to CO_2. This sample was also analyzed in TPD mode. The spectra (not shown here) resemble those shown in Fig. 10a. The presence of coke deposits on the catalysts is again evidenced. The relatively high combustion temperature of these deposits may also suggest that coke is on the bulk of the zeolite and not associated with the platinum phase. In fact, coke deposited on platinum or very close to platinum decomposes below 300 °C due to the catalytic effect of metal [36,37].

Recently, García-Cortés et al. [5] stressed the role of acidic supports in HC-SCR over Pt catalysts by assisting propene adsorption; this reinforces HC-SCR activity on the Pt clean-off step. Also, Yazawa et al. [38–40] have shown the effect of acid strength of support materials on the propane combustion over Pt catalysts. The catalytic activity increases with the acid strength, the explanation found was an enhancement of the oxidation resistance of the platinum in the acid-support materials. Their results corroborate with our hypothesis.

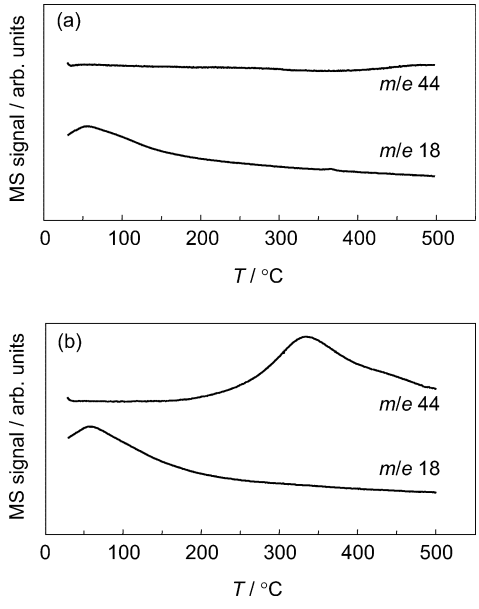

Fig. 10. CO_2 (m/e 44) and H_2O (m/e 18) profiles during TPO of (a) Pt-beta(*c*-0.5) and (b) Pt-beta(*lt*-0.5) samples.

3.5. Effect of the Pt particle size on the deNO$_x$ activity

In this work, Pt-beta catalysts with a wide interval of average metallic particle size have been obtained but excluding the possible effects of other parameters (support, metal loading, and precursor) on the catalytic performance [5]. Differences in the structure of the Pt phase were obtained by applying different heating rates during activation of the ion-exchanged catalyst and upon deNO$_x$ HC-SCR. The increase of the average platinum particle-size has a positive effect on the catalyst activity as shown in Fig. 11a, while it has no effect on the N_2 selectivity. These results confirm the observation of other authors who found an increase of the turnover frequency (expressed as mole NO reduced per mole of surface Pt atom and per second) comparing samples of different nature with different dispersions [4,11,15]. From Fig. 11a, the relatively high activity shown by the smallest platinum particles which must be related to the presence of some big particle, as detected by HRTEM is noted. In Fig. 11b a remarkable linear relationship between particle size and TOF is shown.

One aspect that needs to be elaborated is the presence of highly dispersed irreducible Pt(II) species on the catalysts. In view of this, it is likely that these species do not participate in the deNO$_x$ HC-SCR reaction. XPS, XRD, and HRTEM indicate the transformation of these species into metallic Pt particles in parallel to the growth of the average particle size, which is equivalent to an increasing number of active sites. Reaction with high-temperature-treated samples (*ht-x*) leads

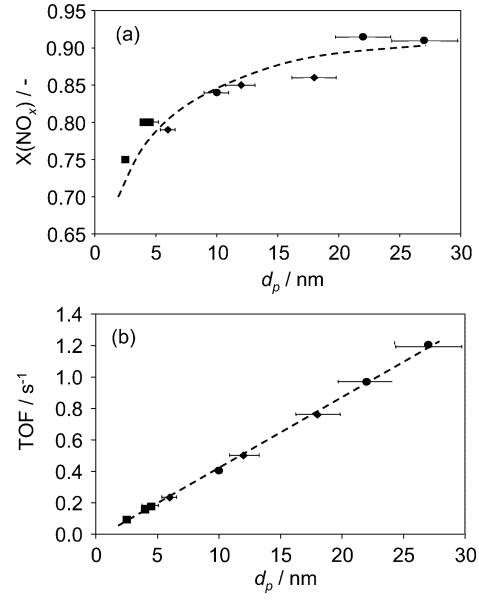

Fig. 11. Correlation between (a) the NO_x conversion and (b) the turnover frequency with the average platinum particle size from CO chemisorption for (■) Pt-beta(*r*), (◆) Pt-beta(*lt*), and (●) Pt-beta(*ht*) at different heating rates.

to the highest activity (Table 2) and at the same time to the highest percentage of surface Pt(0) (Table 3). This phenomenon is, however, not a sufficient explanation for activation by sintering, because from the results in these tables one concludes that catalysts with lower Pt(0) concentrations at the catalyst surface are more active than samples with higher Pt(0) concentrations (compare, e.g., Pt-beta(*r*-0.5) with Pt-beta(*ht*-5)). This stresses the structure sensitivity of HC-SCR over Pt-beta, which is related to the Pt metal particles.

The rate-limiting step of the HC-SCR reaction over Pt metal sites might be related to the oxygen clean-off step or to the NO dissociation step [41,42]. Thus, the HC-SCR activity of a particular Pt metal surface site can be determined, e.g., by its atomic oxygen adsorption enthalpy or by its NO dissociation activity.

Considering different types of surface sites on Pt metal particles and their implication for particle-size dependency, one can discuss various factors. First, different crystallographic planes are present on a Pt particle. Elementary steps on Pt terrace sites can show large crystallographic anisotropies, e.g., for the interaction with NO [43,44]. Atomic nitrogen and oxygen exist on the Pt(100) surface exposed to NO at room temperature while most NO adsorbs molecularly on Pt (110) and (111) [44]. Also desorption temperature of NO strongly depends on the surface orientation of Pt [43,44]. N_2O is formed mainly from NO molecularly adsorbed and N_2 from NO dissociatively adsorbed. The relationship between particle size and different surface sites for platinum particles with a cubo-octahedral structure, following the analysis of van Hardeveld et al. [45–47], was presented by Kinoshita [48]. In the range of Pt particle size of the catalysts studied, the number of Pt atoms on Pt(100) and Pt(111) crystal faces considerably decreases as represented in Fig. 12. As a consequence the number of Pt atoms on the more active plane (100) cannot explain our results.

Secondly, corner and edge sites bind oxygen atoms more strongly than terrace sites [49], which may slow down the oxygen clean-off step. At Pt particle sizes below 10 nm the fractions of corner and edge sites with respect to total number of Pt metal surface sites are strongly dependent on the particle size decreasing with increasing particle size. Above this size the influence is much reduced. Therefore, this will explain the increase in activity observed in catalyst with particle sizes below 10 nm but not above this value.

Based on the previous analysis, it is concluded that referring the HC-SCR activity exclusively to the *number* of specific active sites is not sufficient to explain extremely high TOF on large Pt crystals (in particular (*ht-x*) catalysts). We thus postulate that in this case, a modification of the active sites occurs. Since the number of active sites does not increase, it rather decreases, the specific activity *per site* (probably with a particular structure) must be increased upon reaction. In this sense, it is interesting to point out the phase transition from (hex) to (1×1) examined quantitatively through model simulation and comparison with experiments by Cho [42] in Pt-ZSM-5 in $(NO + C_2H_4 + O_2)$ reaction

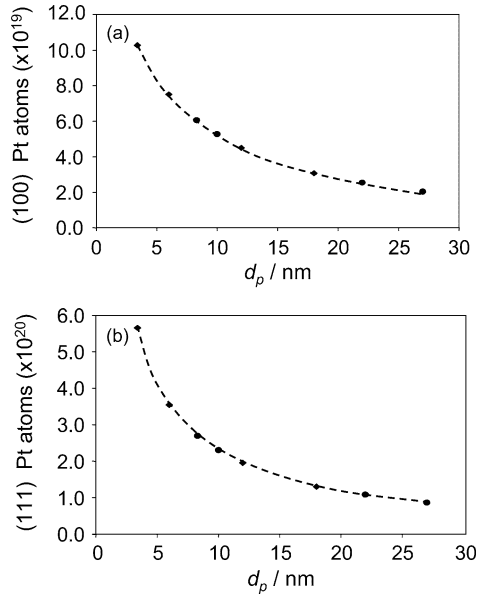

Fig. 12. Correlation between the number of platinum atoms on (a) Pt(100) and (b) Pt(111) planes and the average platinum particle size (after Ref. [48]).

mixture. Phase (1×1) is thermodynamically less stable but more active for NO dissociation [43]. At the moment, no experimental evidence can be provided for the transformation of (hex) to (1×1) phase in our catalysts but it likely to occur upon reaction at high temperature. Further research will be needed to support this hypothesis.

On the other hand, the N_2 selectivity is not affected by Pt particle size. The N_2 selectivity is dependent of the ratio NO dissociatively adsorbed ($N^* + O^*$) to NO molecularly adsorbed (NO^*) [8,50,51]. As Pt(100) can produce atomic nitrogen out of NO ($^*N$) and Pt(111) adsorbs molecular NO ($^*NO$), the particle size-independent Pt(100)/Pt(111) ratio could explain the particle size independence of N_2 selectivity, which is dependent on the $^*N/^*NO$ ratio.

4. Conclusions

Pt-beta catalysts with different metal dispersions have been successfully obtained by applying different heating rates during the activation of ion-exchanged sample by calcination and reduction. Platinum particle size increases with the heating rate, especially from 2 to $5\,^\circ C\,min^{-1}$. Pt-beta catalysts are effective for the selective catalytic reduction of NO_x by propene under excess of oxygen with a N_2 selectivity of 35% and no observable deactivation. An important sintering process of the metal phase, observed by CO chemisorption, HRTEM, and XRD, occurs during the deNO_x reaction. The extent of the sintering process is influenced, as expected, by temperature but more significantly under the effect of the reaction atmosphere. Moreover, the catalysts are activated by sintering of Pt particles, yielding higher NO_x conversions. During reaction, platinum remains

in both oxidized and reduced states evidence of a redox-type reaction pathway. Coke deposits formed during reaction were studied by XPS, DRIFT, and TPO-TPD/MS. These deposits are located in the bulk of the zeolite support rather than associated to the platinum phase.

A correlation between platinum particle size and TOF has been established, confirming the structure sensitivity of the lean deNO_x reaction toward the platinum phase. Large Pt particles show higher activities. Based on our experimental results and previous works with single crystals, it is concluded that structure sensitivity is responsible for greatest ease of the Pt–O clean-off step as corner and edge sites disappear in favor of terrace sites and the larger activity for the NO dissociation step when the Pt(100) hexagonal phase is reconstructed as the (1×1) phase upon reaction. The N_2 selectivity is not affected by the platinum dispersion because N_2O is formed mainly from NO molecularly adsorbed on Pt(111) and N_2 from NO dissociatively adsorbed associated to Pt(100). As the ratio Pt(100)/Pt(111) is almost constant with increasing Pt particle size, the selectivity remains constant.

Acknowledgments

This study was financially supported by MCYT (PPQ 2002-01025) and the Council for Chemical Science of the Netherlands Organisation for Scientific Research (CW-NWO). Dr. Cacciaguerra (Centre de Recherche sur la Matière Divisée, Orleans, France) is gratefully acknowledged for performing the TEM experiments. The authors are indebted to J.C. Groen and N.M. van der Pers for performing the CO chemisorption and XRD experiments, respectively.

References

[1] Y. Traa, B. Burger, J. Weitkamp, Micropor. Mesopor. Mater. 30 (1999) 3.
[2] J. Pérez-Ramírez, J.M. García-Cortés, F. Kapteijn, G. Mul, J.A. Moulijn, C. Salinas-Martínez de Lecea, Appl. Catal. B 29 (2001) 285.
[3] R.J. Farrauto, R.M. Heck, Catal. Today 51 (1999) 351.
[4] R. Burch, P.J. Millington, Catal. Today 26 (1995) 185.
[5] J.M. García-Cortés, J. Pérez-Ramírez, M.J. Illán-Gómez, F. Kapteijn, J.A. Moulijn, C. Salinas-Martínez de Lecea, Appl. Catal. B 30 (2001) 399.
[6] K. Otto, H.C. Yao, J. Catal. 66 (1978) 229.
[7] M.C. Demicheli, L.C. Hoang, J.C. Menezo, J. Barbier, M. Pinabiau, Appl. Catal. A 97 (1993) L11.
[8] I. Balint, A. Miyazaki, K. Aika, Appl. Catal. B 37 (2002) 217.
[9] E. Xue, K. Seshan, J.R.H. Ross, Appl. Catal. B 11 (1996) 65.
[10] T.F. Garetto, C.R. Apesteguia, Catal. Today 62 (2000) 189.
[11] P. Denton, A. Giroir-Fendler, H. Praliaud, M. Primet, J. Catal. 189 (2000) 410.
[12] P. Lööf, B. Stenbom, H. Norden, B. Kasemo, J. Catal. 144 (1993) 60.
[13] S. Schneider, D. Bazin, F. Garin, G. Maire, M. Capelle, G. Meunier, R. Noirot, Appl. Catal. A 189 (1999) 139.
[14] S. Schneider, D. Bazin, G. Meunier, R. Noirot, M. Capelle, F. Garin, G. Maire, Catal. Lett. 71 (2001) 155.
[15] M. Xin, I.C. Hwang, D.H. Kim, S.I. Cho, S.I. Woo, Appl. Catal. B 21 (1999) 183.
[16] H.K. Shin, H. Hirabayashi, H. Yahiro, M. Watanabe, M. Iwamoto, Catal. Today 26 (1995) 13.
[17] E.J. Creyghton, A.C.T. van Duin, J.C. Jansen, P.J. Kooyman, H.W. Zandbergen, H. van Bekkum, J. Chem. Soc., Faraday Trans. 92 (1996) 4637.
[18] F. Delannay, Characterization of Heterogeneous Catalysts, Dekker, New York, 1984.
[19] P. Gallezot, I. Multin, G. Dalmai-Imelik, B.J. Imelik, J. Microsc. Spectrosc. Electron. 1 (1976) 1.
[20] J. de Graaf, A.J. van Dillen, K.P. de Jong, D.C. Koningsberger, J. Catal. 203 (2001) 307.
[21] J.M. Thomas, W.J. Thomas, Principles and Practice of Heterogeneous Catalysis, Wiley–VHC, Germany, 1997.
[22] B.F. Chmelka, G.T. Went, R. Csencsits, A.T. Bell, E.E. Petersen, C.J. Radke, J. Catal. 144 (1993) 507.
[23] V.I. Pârvulescu, P. Grange, B. Delmon, Catal. Today 46 (1998) 233.
[24] M.K. Oudenhuijzen, P.J. Kooyman, B. Tappel, J.A. van Bokhoven, D.C. Koningsberger, J. Catal. 205 (2002) 135.
[25] M.A. Arribas, F. Márquez, A. Martínez, J. Catal. 190 (2000) 309.
[26] J.P. Coutures, R. Erre, D. Massiot, C. Landron, D. Billard, G. Peraudeau, Radiat. Effects 98 (1986) 83.
[27] S. Contarini, S.P. Howlett, C. Rizz, B.A. de Angelis, Appl. Surf. Sci. 51 (1991) 177.
[28] K.H. Ernst, J. Patscheider, R. Hauert, M. Tobler, Surf. Interf. Anal. 21 (1994) 32.
[29] G. Nanse, E. Papirer, P. Fioux, F. Moguet, A. Tressaud, Carbon 35 (1997) 175.
[30] J. Ryczkowski, Catal. Today 68 (2001) 263.
[31] T. Chafik, S. Kameoka, Y. Ukisu, T. Miyadera, J. Mol. Catal. A 136 (1998) 203.
[32] F.C. Meunier, J.P. Breen, V. Zuzaniuk, M. Olsson, J.R.H. Ross, J. Catal. 187 (1999) 493.
[33] T. Okuhara, Y. Hasada, M. Misono, Catal. Today 35 (1997) 83.
[34] W.E.J. van Kooten, H.C. Krijnsen, C.M. van den Bleek, H.P.A. Calis, Appl. Catal. B 25 (2000) 125.
[35] G. Ertl, H. Knozinger, J. Weitkamp, Handbook of Heterogeneous Catalysis, Wiley–VCH, Germany, 1997.
[36] R.A. Comelli, S.A. Canavese, C.A. Querini, N.S. Fígoli, Appl. Catal. A 182 (1999) 275.
[37] D. Duprez, M. Hadj-Aissa, J. Barbier, Appl. Catal. 49 (1989) 67.
[38] Y. Yazawa, H. Yoshida, S. Komai, T. Hattori, Appl. Catal. A 233 (2002) 113.
[39] Y. Yazawa, N. Tagaki, H. Yoshida, S. Komai, A. Satsuma, T. Tanaka, S. Yoshida, T. Hattori, Appl. Catal. A 233 (2002) 103.
[40] Y. Yazawa, H. Yoshida, T. Hattori, Appl. Catal. A 237 (2002) 139.
[41] R. Burch, J.A. Sullivan, T.C. Walting, Catal. Today 42 (1998) 13.
[42] B.K. Cho, J. Catal. 178 (1998) 395.
[43] R.J. Gorte, L.D. Schmidt, J.L. Gland, Surf. Sci. 109 (1981) 367.
[44] S. Sugai, K. Takeuchi, T. Ban, H. Miki, K. Kawasaki, T. Kioka, Surf. Sci. 282 (1993) 67.
[45] R. van Hardeveld, F. Hartog, Surf. Sci. 4 (1966) 396.
[46] R. van Hardeveld, F. Hartog, Surf. Sci. 15 (1969) 189.
[47] R. van Hardeveld, F. Hartog, Advance in Catalysis, Academic Press, New York, 1972.
[48] K. Kinoshita, Electrochemical Oxygen Technology, Wiley, New York, 1992.
[49] H. Wang, R.G. Tobin, D.K. Lambert, C.L. DiMaggio, G.B. Fisher, Surf. Sci. 372 (1977) 267.
[50] R. Burch, A. Ramli, Appl. Catal. B 15 (1998) 49.
[51] R. Burch, A. Ramli, Appl. Catal. B 15 (1998) 63.